



Correction and verification of HL-2A Tokamak Bonner sphere spectrometer in monoenergetic neutron fields from 100 keV to 5 MeV

Bo-Wen Zheng^{1,2} · Chun-Yu Jiang^{1,2} · Zi-Hao Liu^{1,2} · Yin-Hai Pan^{1,2} · Xian-Ying Song³ · Shi-Biao Tang^{1,2} · Ze-Jie Yin^{1,2}

Received: 7 March 2019 / Revised: 4 June 2019 / Accepted: 6 June 2019 / Published online: 21 October 2019

© China Science Publishing & Media Ltd. (Science Press), Shanghai Institute of Applied Physics, the Chinese Academy of Sciences, Chinese Nuclear Society and Springer Nature Singapore Pte Ltd. 2019

Abstract A real-time Bonner sphere spectrometer (BSS) has been developed for spectral neutron measurements with the HL-2A Tokamak. To correct and verify the accuracy of the neutron spectrum from the BSS, the BSS system was calibrated using monoenergetic neutron beams in the energy range of 100 keV–5 MeV. The response function of the BSS was corrected based on the calibration results, and the corrected BSS system was verified by unfolding monoenergetic neutron spectra. Fusion neutron spectra on the HL-2A have been obtained from the calibrated BSS system for the first time.

Keywords Bonner sphere spectrometer · Calibration · Response function · Neutron spectrometry

1 Introduction

The measurement and acquisition of the neutron spectrum and fluence around Tokamak facilities, such as the TFTR [1], JET [2], JT-60U [3], and KSTAR [4], are essential. With the rapid development of the HL-2A, the

first large controlled fusion experimental device with an operating divertor and elongated plasma cross section in China [5–7], developed at the Southwestern Institute of Physics, the fusion neutron spectrum measurements of the HL-2A have received increased interest. These measurements can reflect crucial plasma properties in fusion reactions, such as the reactivity of local deuterium–deuterium (D–D) and deuterium–tritium (D–T) reactions, fuel temperature, and densities [8]. All these parameters are important for estimating the conditions of burning plasma and controlling nuclear reactions inside the plasma. Moreover, the measurement of the fusion neutron near the Tokamak provides the neutron dose in the experimental hall.

Neutron detection at HL-2A has been performed with the consideration of two main factors. One is the strong gamma ray emission around the Tokamak. The other relates to the moderation of the fusion neutron caused by the Tokamak shell, which leads to an extension of the neutron energy to the thermal domain, although the typical fusion neutron energy is 2.45 MeV from the D–D reaction and 14.07 MeV from the D–T reaction. Therefore, the BSS [9], which is known for its relatively high sensitivity to neutrons and wide energy range from thermal to GeV, has been chosen for fusion neutron spectrum measurements on the HL-2A. A typical BSS is made up of several Bonner spheres (BSs), with each BS consisting of a spherical polyethylene moderator and a central thermal neutron detector, such as a ³He or BF₃ proportional counter. The sensitivity of each BS peak at different neutron energy values depends on its diameter [10]. As a result, we can derive the neutron spectrum in the measured field from the measured count rates of a set of BSs. Here, the mathematical principle of the BSS is described. If sphere *i* has

This work was supported by the National Natural Science Foundation of China (Nos. 11375195 and 11575184).

✉ Bo-Wen Zheng
myzbw@mail.ustc.edu.cn

¹ State Key Laboratory of Particle Detection and Electronics, University of Science and Technology of China, Hefei 230026, China

² Department of Modern Physics, University of Science and Technology of China, Hefei 230026, China

³ Southwestern Institute of Physics, Chengdu 610041, China

response function $R_i(E)$ and is exposed in a neutron field with spectral fluence $\phi(E)$, the reading of the sphere N_i is obtained by folding $R_i(E)$ with $\phi(E)$:

$$N_i = \int R_i(E)\phi(E)dE. \tag{1}$$

After discretization, Eq. (1) becomes:

$$N_i = \sum_{j=1}^n R_{ij}\phi_j, \tag{2}$$

and j is the index over discrete energy points. With m BSs, R_{ij} is an $m \times n$ response matrix, which is calculated in advance. After acquiring the BS reading N_i , we can obtain the neutron spectrum by solving the set of m linear equations in Eq. (2). However, for a limited number of BSs ($m < n$), Eq. (2) becomes an underdetermined problem, which can only be solved by mathematical unfolding algorithms.

In this study, the real-time BSS system on the HL-2A is described, as is the calculation of its response function. On the basis of previous validation experiments using a $^{241}\text{Am-Be}$ neutron source [11], the BSS system was calibrated on monoenergetic neutron beams in the energy range of 100 keV–5 MeV. According to the calibration results, the response function of BSS was improved and corrected to obtain the precise neutron spectrum from the BS reading. The modified response function was then verified by unfolding the monoenergetic neutron spectra. After correction and verification of the BSS system, the fusion neutron spectrum on the HL-2A was obtained from the calibrated BSS system.

2 Bonner sphere spectrometer and response function

2.1 Bonner sphere spectrometer system

The HL-2A BSS system consists of a set of eight polyethylene spheres (density $\rho_{\text{PE}} = 0.946 \text{ g/cm}^3$) with diameters of 3, 5, 7, 8, 9, 10, 12, and 15 in a high-voltage supply, an eight-channel pre-amplifier, a data acquisition system (DAQ), and a host computer. Figure 1 shows the

structure of the BSS system. The active part of the BSS is a ^3He proportional counter (model SP9, Centronic Ltd. UK) with a diameter of 33 mm for the spherical part, which is located in the central cavity of each BS. The counter is filled with 2 atm of ^3He gas.

With respect to the electronics, we have developed a new electronics system for the BSS to meet the real-time requirements of the HL-2A [12]. The operating high voltage for the BS is 900 V, reaching a neutron sensitivity of 8 cps, yielding 3.2 mrem/h. The signal processing procedure is simply described here. First, the pulses from eight counters are synchronously amplified using the eight-channel pre-amplifier, with a voltage charge ratio of $2 \times 10^{14} \text{ V/C}$. Then, the DAQ rejects the pulses due to gamma particles and electronic noise. Finally, the FPGA acquires eight real-time channel neutron counts and uploads them to the host computer for spectrum unfolding. The DAQ consists of a comparator, a DAC, and an FPGA. Because of the different pulse height distribution of neutrons, gamma rays, and noise, a discriminator threshold is used to select neutron signals. The threshold value is set by the host computer, received by the FPGA, converted to an analog signal by the DAC, and finally, sent to the comparator. For the internal parallel processing characteristics of the FPGA, the eight-channel signals can be collected and processed synchronously. Meanwhile, the spectrum unfolding algorithm in the host computer has a computation cost of less than 2 ms. After a field test, the BSS can calculate and show the dynamic measured spectrum after 2 ms [12]. Figure 2 shows a photograph of the BSS system.

2.2 Calculation of the response function

On the basis of previous studies [13], the response function of the BSS was re-calculated in the present study with a larger number of incident neutrons to reduce the statistical uncertainty. The response function was determined with the Monte Carlo tool Geant4 [14] by setting a uniform parallel neutron beam with the same diameter as the BS and colliding the neutron beam with the BS along the ^3He detector cylindrical axis [15]. We simulated 5×10^8 neutrons at 49 energy points in the energy range 10^{-9} –18 MeV. The discrete energy values were selected in

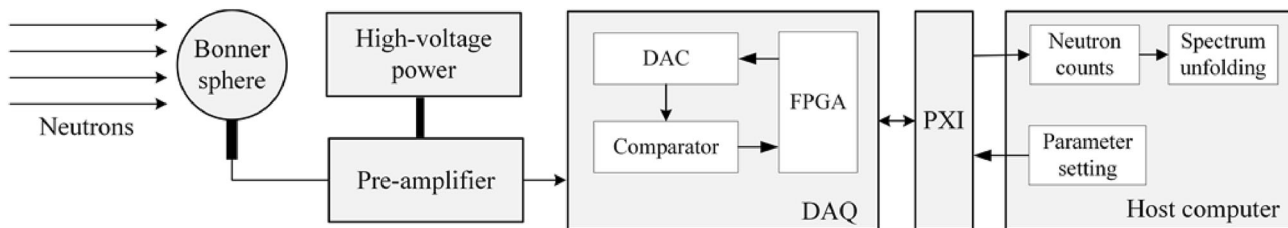


Fig. 1 Schematic diagram of the BSS system structure

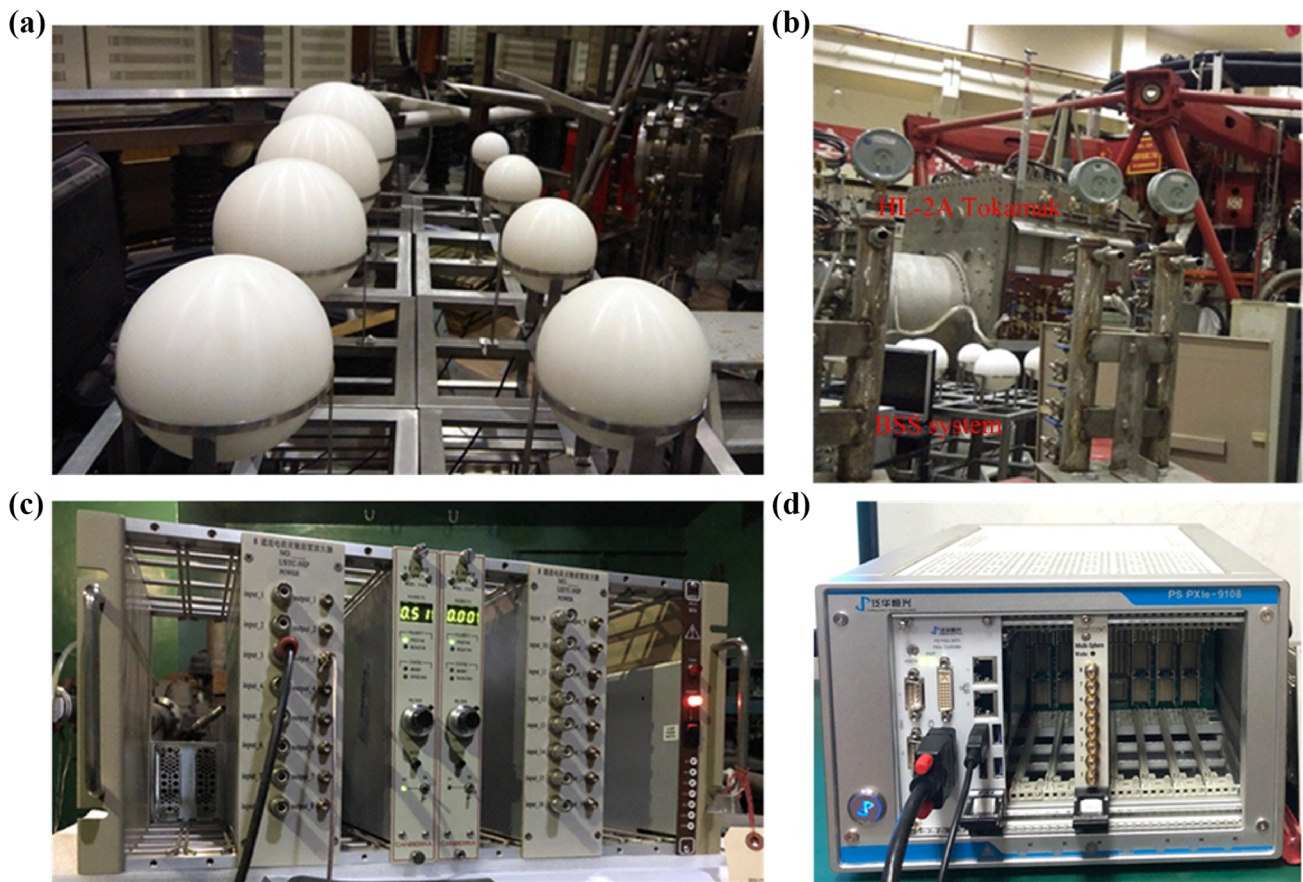


Fig. 2 (Color online) Photograph of the BSS system. **a** Setup of the BSs [12]. **b** Experiment environment on HL-2A. **c** Eight-channel pre-amplifier. **d** DAQ system

the logarithmic domain with equal intervals from 10^{-9} to 10^0 MeV. Meanwhile, in the range between 1 MeV and 20 MeV, more points were chosen to show the detailed structure of its peak [13]. Table 1 shows the physical model used in the Geant4 simulation. Here, we define the response function as neutron counts in ^3He per incident neutron. Figure 3 shows the calculated response function,

and its relative statistical uncertainty is below 1.7%. As expected, the response function peak gradually moves to a higher energy range as the BS diameter increases. The shape of the BSS response function is similar to that of the other BSS systems in the published literature [10, 15–17].

3 Calibration of the BSS at monoenergetic neutron fields

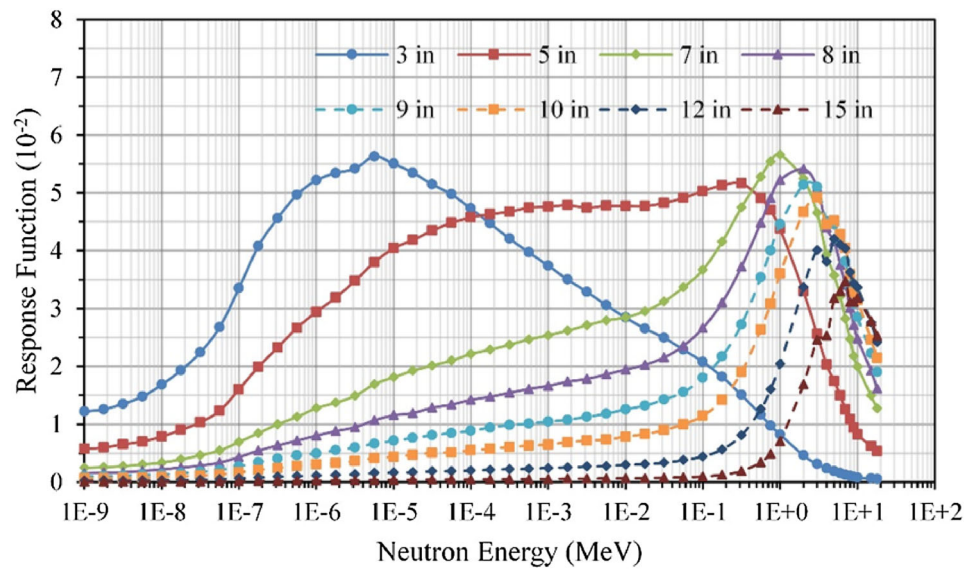
3.1 Calibration measurements

To validate the calculated response function at precise energies, calibration measurements were carried out in the low-scatter irradiation room of the Institute of Nuclear Science and Technology, Sichuan University [18, 19], using a 2.5-MV Van de Graaff accelerator. According to the international standard ISO 8529-1 for the calibration of detectors, a full set of eight BSs were used in the experiment at neutron energies of 122 keV, 352 keV, 582 keV, 1 MeV, 3.65 MeV, and 4.70 MeV. Monoenergetic neutron beams were produced by nuclear reactions induced by protons or deuterons, on tritium–titanium (T–Ti) or

Table 1 Physical model selected for different physical processes in the Geant4 simulation [13]

Physical process	Energy range	Physical model
Elastic scatter	< 4 eV	NeutronHPThermalScattering
	4 eV–20 MeV	NeutronHPElastic
	> 20 MeV	hElasticCHIPS
Inelastic scatter	< 20 MeV	NeutronHPInelastic
	> 20 MeV	Binary Cascade
Neutron capture	< 20 MeV	NeutronHPCapture
	> 20 MeV	nRedCapture
Neutron fission	< 20 MeV	NeutronHPFission
	> 20 MeV	G4LFission

Fig. 3 (Color online) Response functions for the HL-2A Tokamak BSS simulated by Geant4



deuterium–titanium (D–Ti) targets. All measurements were performed by exposing the BS to neutrons emitted in the selected direction at a distance of 2 m from the neutron-producing target. Table 2 summarizes the main characteristics of the produced neutron beams. The accelerator has a large open geometry experimental hall ($9.75 \times 11.45 \times 3.97 \text{ m}^3$), which minimizes the backscattered neutron, and an ISO 8529 standard shadow cone (SC), used to subtract the scatter contribution from the detector readings. This contribution was in the range of 27–42% for the 3-in BS; meanwhile, the component of the scattered neutron for the largest BS of diameter 15 in was only 5–13%. The difference in the scatter contribution was caused by the small BS having a higher response of low-energy neutrons than that of the large BS. After several elastic scatterings, the energy of the scattered neutrons is quite low. Therefore, the component of scattered neutrons for small BS was higher than that for large BS. The minor influence [16, 20] of the target scattering neutrons was neglected by using the specially made copper pipe and the simplified target unit (particularly the target material and backing) [21]. Furthermore, the reference value of the

monoenergetic neutron fluence delivered to the BS center was known through measurements with the standard BF_3 long counter [19] at 40° with respect to the ion beam and 2.2 m from the target.

3.2 Calibration results

For the eight BSs at the six experimental monoenergetic energy points, the measured response function of the BSS was derived as follows:

$$R_M = \frac{C_{\text{total}}}{\phi_{\text{total}}} - \frac{C_{\text{SC}}}{\phi_{\text{SC}}}, \quad (3)$$

where R_M is the measured response function, C_{total} is the neutron counts of the BS without the shadow cone, ϕ_{total} is the monoenergetic neutron fluence delivered at the BS center without the shadow cone, C_{SC} is the neutron counts of the BS with the shadow cone, and ϕ_{SC} is the monoenergetic neutron fluence delivered at the BS center with the shadow cone.

The R_M calculated from Eq. (3), the Geant4 calculated response R_C , as well as the average ratio of the calculated

Table 2 Main characteristics of the monoenergetic neutron beams used for the calibration of the BSS

Neutron energy (keV)	Reaction	Incident particle energy (MeV)	Measurement angle ($^\circ$)	Standard uncertainty on reference fluence (%)
122	$\text{T}(p, n)^3\text{He}$	1.2	60	± 2.9
352	$\text{T}(p, n)^3\text{He}$	1.2	0	± 2.6
582	$\text{T}(p, n)^3\text{He}$	1.8	60	± 2.3
1000	$\text{T}(p, n)^3\text{He}$	1.8	0	± 2.3
3650	$\text{D}(d, n)^3\text{He}$	1.5	60	± 1.9
4700	$\text{D}(d, n)^3\text{He}$	1.5	0	± 2.3

to measured response function ($f_c = \frac{R_C}{R_M}$) for each BS are listed in Table 3. The first uncertainty of f_c is the standard deviation of the ratio of the calculated to measured response function for all energy points, and the second uncertainty is the total uncertainty after taking the reference fluence in Table 2 into account [22]. Figure 4 shows the ratios of the calculated to measured response function ($\frac{R_C}{R_M}$) at monoenergetic neutron fields based on Table 3.

It is observed from Table 3 that the f_c values for all BSs are larger than 1, which means that the measurements generally give smaller results than the Geant4 calculated response function. This may result from detector parameters that were not considered in the Geant4 simulation, which is in accordance with other studies and analyses reported before [20]. It can be calculated from Table 3 and Fig. 4 that the difference between the measured and calculated response function ranges from 0.43 to 16.31%, with an average difference of 7.12%. Compared with the calibration results of other BSS facilities [16, 20, 23], the difference in our BSS is reasonable but higher than the results of BSS at IRSN [22, 24]. With respect to the correction of the response function, we define f_c as a correction factor, and the response function of each BS was corrected by multiplying the reciprocal of f_c by the originally calculated response function. After being corrected,

the modified f_c value for each BS was 1.00, which means that the average deviation of the calculated response function from the measured response function had been improved, and the corrected response function was available for the spectrum unfolding process. Figure 5 shows the absolute differences between the corrected and Geant4 calculated response functions.

4 Verification of the BSS system

4.1 Monoenergetic neutron spectra unfolding

Once the final BSS response function was constructed, six neutron spectra representing the monoenergetic neutron sources were measured and unfolded. The measurements were performed under the same experiment conditions as those of the calibration experiment; in other words, six neutron spectra were measured using the neutron beams described in Table 2 and the shadow cone subtraction method. The accuracy of the integral dose equivalent [25] is within 10%. According to Eq. (2), mathematical algorithms should be used to obtain non-unique solutions for the equations [26–28]. In this study, the least-squares method (LSM) was utilized for the unfolding procedure [29], and the LSM unfolding algorithm was verified by a

Table 3 Measured and calculated response function at standard monoenergetic neutron fields

Energy (keV)	3 in		5 in		7 in		8 in	
	R_M	R_C	R_M	R_C	R_M	R_C	R_M	R_C
122	1.26×10^{-2}	1.40×10^{-2}	4.25×10^{-2}	4.52×10^{-2}	3.06×10^{-2}	3.43×10^{-2}	2.17×10^{-2}	2.49×10^{-2}
352	1.32×10^{-2}	1.33×10^{-2}	4.55×10^{-2}	5.24×10^{-2}	4.90×10^{-2}	4.97×10^{-2}	3.50×10^{-2}	3.97×10^{-2}
582	7.77×10^{-3}	8.35×10^{-3}	4.71×10^{-2}	4.56×10^{-2}	4.33×10^{-2}	4.98×10^{-2}	4.03×10^{-2}	4.25×10^{-2}
1000	2.83×10^{-3}	2.49×10^{-3}	4.73×10^{-2}	4.23×10^{-2}	5.97×10^{-2}	5.68×10^{-2}	4.63×10^{-2}	5.19×10^{-2}
3650	2.55×10^{-3}	2.35×10^{-3}	2.33×10^{-2}	2.34×10^{-2}	4.19×10^{-2}	4.40×10^{-2}	4.30×10^{-2}	4.81×10^{-2}
4700	1.59×10^{-3}	1.80×10^{-3}	1.41×10^{-2}	1.64×10^{-2}	3.31×10^{-2}	3.38×10^{-2}	3.51×10^{-2}	3.86×10^{-2}
f_c	$1.02 \pm 9.4\%$ $\pm 9.8\%$		$1.04 \pm 9.6\%$ $\pm 10.0\%$		$1.05 \pm 6.7\%$ $\pm 7.3\%$		$1.11 \pm 3.0\%$ $\pm 4.2\%$	
Energy (keV)	9 in		10 in		12 in		15 in	
	R_M	R_C	R_M	R_C	R_M	R_C	R_M	R_C
122	1.86×10^{-2}	1.69×10^{-2}	9.62×10^{-3}	1.11×10^{-2}	3.71×10^{-3}	4.27×10^{-3}	8.66×10^{-4}	9.08×10^{-4}
352	2.87×10^{-2}	2.94×10^{-2}	1.79×10^{-2}	2.05×10^{-2}	7.09×10^{-3}	8.16×10^{-3}	1.93×10^{-3}	2.08×10^{-3}
582	2.91×10^{-2}	3.28×10^{-2}	2.03×10^{-2}	2.26×10^{-2}	8.51×10^{-3}	9.76×10^{-3}	2.10×10^{-3}	2.17×10^{-3}
1000	3.92×10^{-2}	4.31×10^{-2}	2.99×10^{-2}	3.35×10^{-2}	1.46×10^{-2}	1.63×10^{-2}	2.55×10^{-3}	2.32×10^{-3}
3650	4.58×10^{-2}	4.90×10^{-2}	4.16×10^{-2}	4.69×10^{-2}	3.49×10^{-2}	3.90×10^{-2}	2.22×10^{-2}	2.46×10^{-2}
4700	3.95×10^{-2}	4.11×10^{-2}	3.81×10^{-2}	4.21×10^{-2}	3.57×10^{-2}	3.81×10^{-2}	2.57×10^{-2}	2.81×10^{-2}
f_c	$1.05 \pm 7.0\%$ $\pm 7.6\%$		$1.12 \pm 1.7\%$ $\pm 3.4\%$		$1.13 \pm 3.0\%$ $\pm 4.2\%$		$1.05 \pm 6.6\%$ $\pm 7.2\%$	

Fig. 4 (Color online) Ratios of the calculated to measured response function (R_C/R_M) for 122, 352, 582 keV, and 1, 3.65, 4.70 MeV monoenergetic neutron sources

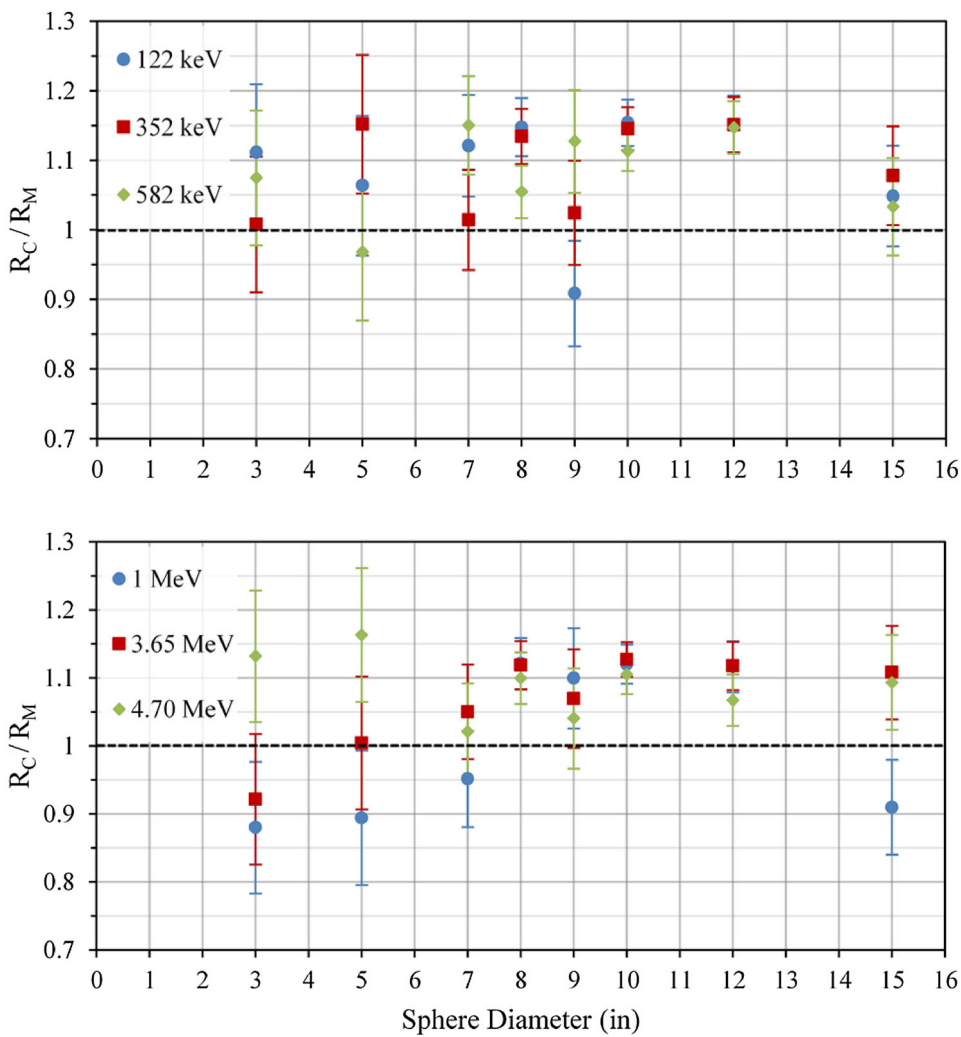
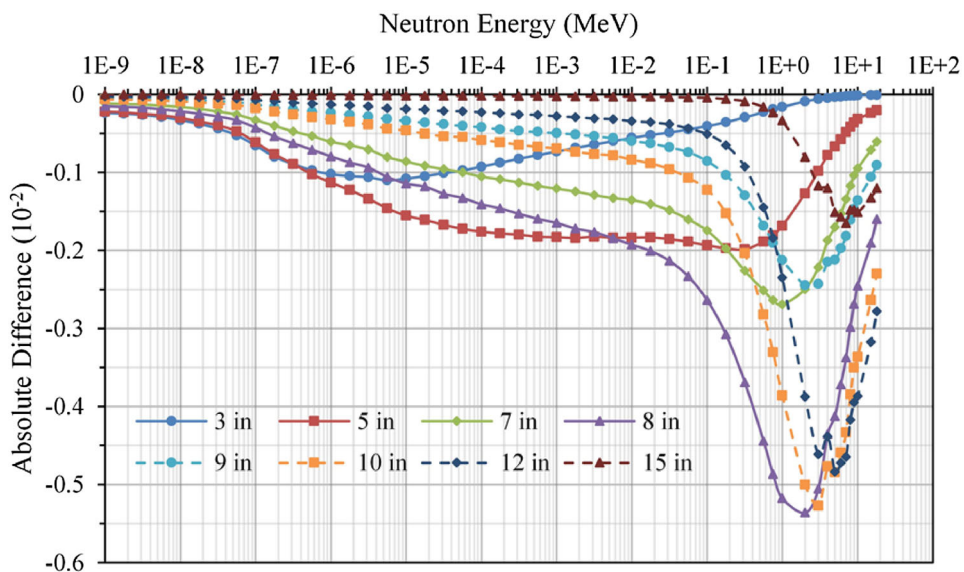


Fig. 5 (Color online) Absolute differences between the corrected and Geant4 calculated response functions



standard ^{241}Am -Be neutron source [11]. The main idea of the LSM is to minimize the squared residual error of Eq. (2), which means that the solution when folded back should match the measured data within the minimum error. The spectra were unfolded with a user-defined priori spectrum [30], the neutron counts of the BSS at the monoenergetic neutron beams, final corrected response function, and LSM algorithm. Figure 6 shows the unfolded intensity spectra, and the process is performed iteratively.

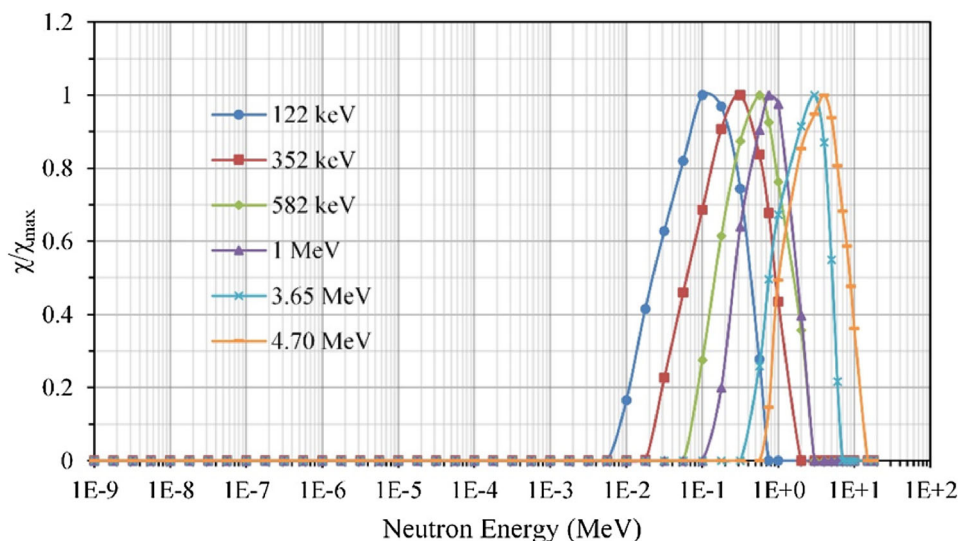
As the response function spans the energy interval from 10^{-9} to 20 MeV in 48 bins, the total sensitive energy region of the neutron spectrum is also the same. Clear peak shapes are observed in the spectra in Fig. 6 [30], with peaks at 100, 316, 562, 750, 3000, and 4000 keV. The energy peak values in the unfolded spectra deviate from the energies of the monoenergetic neutrons, owing to the following reasons. First, the response function was calculated for the energy range of 10^{-9} to 1 MeV and for energies above 1 MeV, considering four energies per decade of energy and each integer energy point, respectively. Therefore, the spectra unfolded on discrete energy points inevitably deviated from the actual monoenergetic neutron field. Second, because of the energy spread of the neutron beams, the energy of the neutrons detected by BS was lower than expected, as calculations revealed that the energy spread of the neutron beams was less than 2.59%. Figure 6 shows that the energy peak values in the unfolded spectra are all a bit lower than those of the neutron beams, and these spectra always peak at the lower energy points that are nearest to the energy of the neutron beams. Taking these above factors into account, the unfolded neutron spectra at monoenergetic neutron beams are basically correct, and our BSS with the corrected response function is reliable and practical.

4.2 Results of the measurement on HL-2A

This calibrated and corrected BSS has been applied to neutron measurements on the HL-2A for the first time. Figure 2 shows the experimental environment, with eight BSs placed in two parallel rows 40 cm apart and the vertical distance between the BSS and the outer wall of the Tokamak of 5.4 m. Major parameters for the HL-2A are as follows: R (major radius) = 1.65 m, a (minor radius) = 0.4 m, I_p (plasma current) = 480 kA, and P_{NBI} (neutral beam power) = 1 MW [6]. Neutrons with an energy of 2.45 MeV were generated by the D–D fusion reaction inside the vacuum vessel. Figure 7 is the measured data of one plasma discharge process #28935. The plasma current in the vacuum vessel increased from 0 ms and remained stable near 160 kA. The neutral beam injection (NBI) occurred at 500 ms, with a power of 700 kW. Once the NBI occurred, the D–D reaction began to produce neutrons, and the eight BS detectors exhibited neutron counts. Figure 7 shows that neutron counts drop lower near 600 ms, and this effect is more visible in smaller BSs. Because the electron cyclotron resonance heating (ECRH) began near 600 ms, the temperature of the plasma electron increased and its density decreased, which led to a decrease in the neutron counts at 600 ms [31]. Based on the neutron counts, the spectra were unfolded on the host computer synchronously. Figures 8 and 9 are the normalized average intensity spectra in 10 ms at different time points during the plasma discharge, and the accuracy of the integral dose equivalent is within 10%.

At the experiment hall, the neutrons produced by the D–D reaction were scattered by the surrounding materials around the Tokamak, which divided the neutron spectrum into the fast and thermal neutron components [32]. Therefore, two peaks in the fast and thermal neutron range

Fig. 6 (Color online) Neutron spectra obtained from the corrected BSS for monoenergetic neutron sources at 122, 352, 582 keV, and 1, 3.65, 4.70 MeV



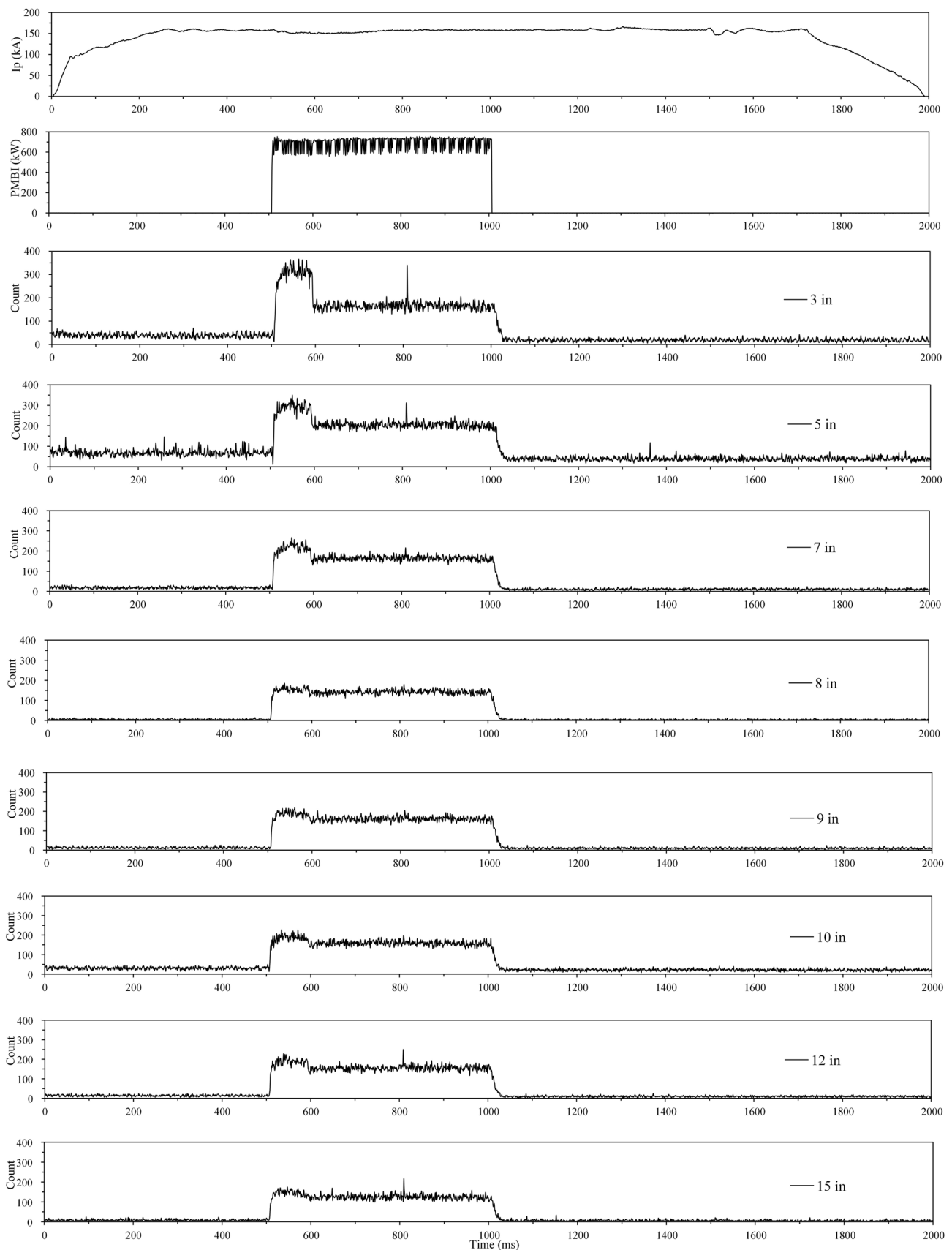


Fig. 7 Time traces of neutral beam power, plasma current, and neutron count rates of eight BS detectors during a plasma discharge (#28935)

Fig. 8 Normalized average intensity spectrum during 550–560 ms of the plasma discharge in the HL-2A experiment hall

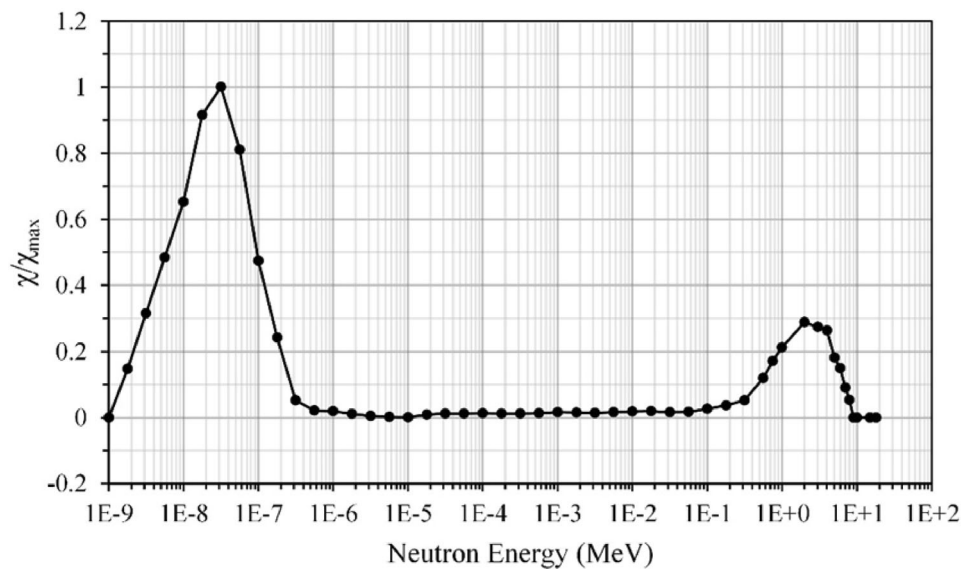
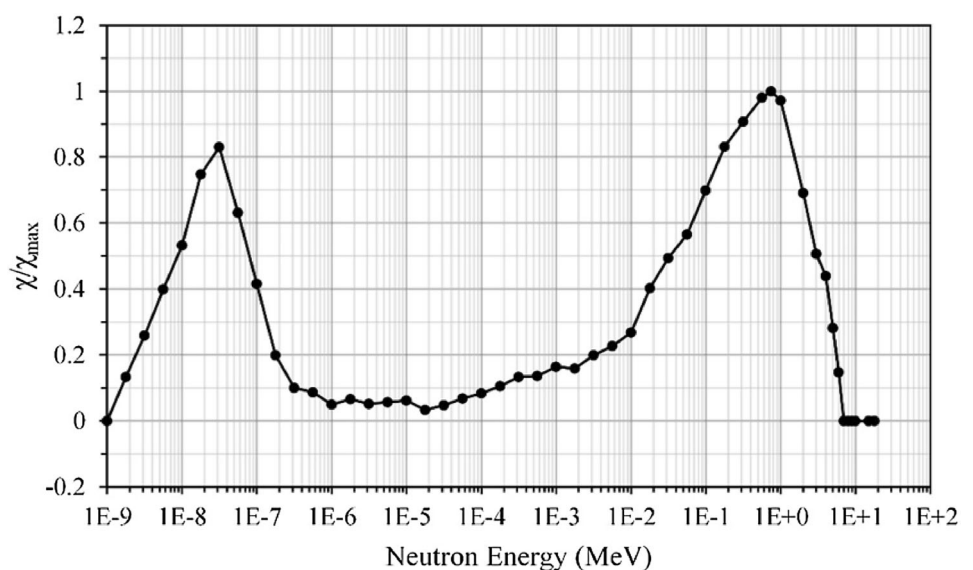


Fig. 9 Normalized average intensity spectrum during 650–660 ms of the plasma discharge in the HL-2A experiment hall



are observed in Fig. 8 and Fig. 9. Both the spectra mentioned above have similarities and distinctions, and they can be divided into three regions. First, neutrons were produced by inelastic scattering in the energy range of 10 keV–2.45 MeV. Second, neutrons were moderated by elastic scattering with materials in the flat energy range of 1 eV to 10 keV. Third, the thermal peak at 31.6 meV was caused by neutrons that were in thermal equilibrium with wall materials at room temperature [12, 32]. Due to the reduction in the neutron count rate near 600 ms, caused by the ECRH, the neutron spectrum changed from Figs. 8 and 9 in the plasma discharge process. The main difference between these two spectra is the energy peak structure in the fast neutron range. The spectrum in Fig. 9 shares a common structure with the D–D neutron spectrum on EAST [32], while the intensity of the fast neutron peak in

Fig. 8 is lower than that of its thermal neutron peak, and the neutron energy of the fast neutron peak is higher than that in Fig. 9. The variation tendency in the neutron spectra observed above can reflect the D–D reaction inside the HL-2A and will be used for the analysis of fusion reactions.

5 Conclusion

The HL-2A BSS response function was calculated using Geant4, and the BSS system was further calibrated in the monoenergetic neutron fields using a Van de Graaff accelerator. Based on the calibration results, the difference between the calculated and measured response function ranges from 0.43 to 16.31%, with an average difference of 7.12%. After being corrected, the average difference

between the calculated and measured response function for each BS reached 0%. To experimentally verify the corrected BSS, measurements of six monoenergetic neutron spectra were taken. A clear structure and expected energy values were observed in all six spectra. The corrected and verified BSS was then used on the HL-2A, and real-time neutron spectra were obtained, allowing further improvement in future nuclear research on HL-2A. This study shows that the BSS is reliable and practical. Future research will include adding more spheres with diameters of 3–5 into show the details of spectrum in thermal neutron range and similar calibration experiments in the 10–20 MeV energy range. The calibration result in the higher energy range will then be applied to correct the response function.

References

- H.W. Kugel, G. Ascione, J. Gilbert, Review of diagnostic methods for TFTR D–T radiation shielding and neutronics studies. *Rev. Sci. Instrum.* **68**, 557 (1997). <https://doi.org/10.1063/1.1147652>
- M.T. Swinhoe, O.N. Jarvis, Measurement and calculation of the efficiency of fission detectors designed to monitor the time dependence of the neutron production of JET. *Rev. Sci. Instrum.* **56**, 1093 (1985). <https://doi.org/10.1063/1.1138233>
- M. Hoek, T. Nishitani, Y. Ikeda et al., Neutron yield measurements by use of foil activation at JT-60U. *Rev. Sci. Instrum.* **66**, 885 (1995). <https://doi.org/10.1063/1.1146527>
- H. Kim, H. Lee, S. Hong et al., Radioactivity evaluation for the KSTAR Tokamak. *Radiat. Prot. Dos.* **116**, 24 (2005). <https://doi.org/10.1093/rpd/nci242>
- D. Liu, C. Zhou, Z. Cao et al., Construction of the HL-2A Tokamak. *Fusion Eng. Des.* **66–68**, 147 (2003). [https://doi.org/10.1016/S0920-3796\(03\)00165-0](https://doi.org/10.1016/S0920-3796(03)00165-0)
- Q. Li, Brief introduction to engineering and experiment of HL-2A Tokamak. *At. Energy Sci. Technol.* **43**, 204 (2009). (in Chinese)
- Y. Liu, X. Ding, Q. Yang et al., Recent advances in the HL-2A Tokamak experiments. *Nucl. Fusion* **45**, S239–S244 (2005). <https://doi.org/10.1088/0029-5515/45/10/S19>
- I. Klimek, M. Cecconello, M. Gorelenkova et al., TRANSP modelling of total and local neutron emission on MAST. *Nucl. Fusion* **55**, 023003 (2015). <https://doi.org/10.1088/0029-5515/55/2/023003>
- R.L. Bramblett, R.I. Ewing, T.W. Bonner, A new type of neutron spectrometer. *Nucl. Instrum. Methods.* **9**, 1 (1960). [https://doi.org/10.1016/0029-554X\(60\)90043-4](https://doi.org/10.1016/0029-554X(60)90043-4)
- D.J. Thomas, A.V. Alevra, Bonner sphere spectrometers: a critical review. *Nucl. Instrum. Methods A.* **476**, 12–20 (2002). [https://doi.org/10.1016/S0168-9002\(01\)01379-1](https://doi.org/10.1016/S0168-9002(01)01379-1)
- J. Cao, C. Jiang, H. Cao et al., Experimental validation of a Tokamak neutron spectrometer based on Bonner spheres. *Chin. Phys. C.* **39**(8), 086001 (2015). <https://doi.org/10.1088/1674-1137/39/8/086001>
- C. Jiang, J. Cao, X. Jiang et al., Real-time bonner sphere spectrometry on the HL-2A Tokamak. *Plasma Sci. Technol.* **18**, 699 (2016). <https://doi.org/10.1088/1009-0630/18/6/19>
- J. Cao, X. Jiang, C. Jiang et al., Calculation of response function for bonner sphere spectrometer based on Geant4. *Plasma Sci. Technol.* **17**, 80 (2015). <https://doi.org/10.1088/1009-0630/17/1/15>
- S. Agostinelli, J. Allison, K. Amako et al., Geant4: a simulation toolkit. *Nucl. Instrum. Methods A.* **506**, 250–303 (2003). [https://doi.org/10.1016/S0168-9002\(03\)01368-8](https://doi.org/10.1016/S0168-9002(03)01368-8)
- R. Bedogni, A. Pola, M. Costa et al., A Bonner sphere spectrometer based on a large $^6\text{LiI(Eu)}$ scintillator: calibration in reference monoenergetic fields. *Nucl. Instrum. Methods A.* **897**, 18–21 (2018). <https://doi.org/10.1016/j.nima.2018.04.040>
- R.M. Howell, E.A. Burgett, B. Wiegel et al., Calibration of a Bonner sphere extension (BSE) for high-energy neutron spectrometry. *Radiat. Meas.* **45**(10), 1233–1237 (2010). <https://doi.org/10.1016/j.radmeas.2010.09.003>
- B. Wiegel, A.V. Alevra, NEMUS: the PTB neutron multisphere spectrometer—Bonner spheres and more. *Nucl. Instrum. Methods A.* **476**, 36–41 (2002). [https://doi.org/10.1016/S0168-9002\(01\)01385-7](https://doi.org/10.1016/S0168-9002(01)01385-7)
- H. Sun, X. Luo, C. Li et al., The measurement of neutron flux using ^{197}Au neutron activation from static accelerator. *Nucl. Electron. Detect. Technol.* **30**, 288–295 (2010). <https://doi.org/10.3969/j.issn.0258-0934.2010.02.032>. (in Chinese)
- Z. Zhu, Y. Hua, W. Chen et al., Efficiency calibration of long counter and its application. *J. Sichuan Univ. (Natural Science Edition)* **52**, 1303 (2015). <https://doi.org/10.3969/j.issn.0490-6756.2015.11.021>. (in Chinese)
- C. Birattari, E. Dimovasili, A. Mitaroff et al., A Bonner sphere spectrometer with extended response matrix. *Nucl. Instrum. Methods A.* **620**, 260–269 (2010). <https://doi.org/10.1016/j.nima.2010.04.033>
- T. Peng, X. Luo, C. Zhang et al., Study on calibration of neutron efficiency and relative photo-yeild of plastic scintillator. *Nucl. Phys. Rev.* **19**(3), 57–60 (2002). <https://doi.org/10.11804/NuclPhysRev.19.03.357>. (in Chinese)
- V. Lacoste, V. Gressier, J.L. Pochat et al., Characterization of Bonner sphere system at monoenergetic and thermal neutron fields. *Radiat. Prot. Dosim.* **110**(1–4), 529–532 (2004). <https://doi.org/10.1093/rpd/nch279>
- T. Ogata, S. Kudo, Y. Watanabe et al., The calibration of Bonner sphere spectrometer. *Radiat. Prot. Dosim.* **146**(1–3), 107–110 (2011). <https://doi.org/10.1093/rpd/ncr123>
- A. Cheminet, V. Lacoste, V. Gressier et al., Characterization of the IRSN neutron multisphere spectrometer (HERMEIS) at European standard calibration fields. *J. Instrum.* **7**, C04007 (2012). <https://doi.org/10.1088/1748-0221/7/04/C04007>
- A. Alevra, D. Thomas, Neutron spectrometry in mixed fields: multisphere spectrometer. *Radiat. Prot. Dosim.* **107**, 37–72 (2003). <https://doi.org/10.1093/oxfordjournals.rpd.a0063848>
- R. Bedogni, C. Domingo, A. Esposito et al., FRUIT: an operational tool for multisphere neutron spectrometry in workplaces. *Nucl. Instrum. Methods A.* **580**, 1301–1309 (2007). <https://doi.org/10.1016/j.nima.2007.07.033>
- M. Matzke, Unfolding procedures. *Radiat. Prot. Dosim.* **107**, 155–174 (2003). <https://doi.org/10.1093/oxfordjournals.rpd.a006384>
- C.S. Zaidins, J.B. Martin, F.M. Edwards, A least-squares technique for extracting neutron spectra from Bonner sphere data. *Med. Phys.* **5**, 42–45 (1978). <https://doi.org/10.1118/1.594464>
- J. Cao, C. Jiang, Q. Yang et al., Verification of a fusion neutron diagnostic Bonner sphere spectrometer on measurement of a ^{241}Am –Be neutron source. *Nucl. Sci. Tech.* **27**, 127 (2016). <https://doi.org/10.1007/s41365-016-0126-2>
- A. Esposito, M. Nandy, Measurement and unfolding of neutron spectra using Bonner spheres. *Radiat. Prot. Dosim.* **110**(1–4), 555–558 (2004). <https://doi.org/10.1093/rpd/nch385>

31. W.Y. Hong, L.W. Yan, K.J. Zhao et al., Experimental observation of divertor configuration and ECRH on the HL-2A Tokamak. *Nucl. Fusion. Plasma. Phys.* **27**(1), 7–11 (2007). <https://doi.org/10.3969/j.issn.0254-6086.2007.01.002>. (in Chinese)
32. Z.M. Hu, X.F. Xie, Z.J. Chen et al., Monte Carlo simulation of a Bonner sphere spectrometer for application to the determination of neutron field in the experimental advanced superconducting Tokamak experimental hall. *Rev. Sci. Instrum.* **85**, 11E417 (2014). <https://doi.org/10.1063/1.4891163>